Relativistic electron transport and beam filamentation in foams

P. A. Wilson, M. Borghesi, L. Romagnani, K. Quinn and B. Ramakrishna
School of Mathematics and Physics, Queen's University Belfast, Belfast BT7 1NN, UK

A. Pipahl and O.Willi
Insitut für Laser-und Plasmaphysik, Heinrich-Heine-Universität, Düsseldorf (D), Germany

L. Lancia and J. Fuchs
Laboratoire pour l'Utilisation des Laser Intenses (LULI) CNRS-Ecole Polytechnique-Univ, Paris, France

R. G. Evans
The Blackett Laboratory, Imperial College of Science, Technology and Medicine, London SW7 2 BZ, UK

W. Nazarov
School of Chemistry, University of St Andrews, St Andrews

R. J. Clarke and M. M. Notley
Central Laser Facility, STFC, Rutherford Appleton Laboratory, HSIC, Didcot, Oxon OX11 0QX, UK

Contact | pwilson22@qub.ac.uk

Introduction

High intensity laser matter interaction results in the production of highly energetic particles. Large relativistic electron currents are produced, exceeding the Alfven limit by a factor of hundreds or thousands. Return currents from the cold plasma are essential to allow propagation of this extremely large relativistic current into the target. The unstable spatial distribution of forward and return current results in electromagnetic of the Weibel type, leading to current filamentation, detrimental to the propagation of fast electrons inside matter.

Transport of fast electrons is a crucial issue in the realization of the Fast Ignition scheme where the fast electron beam is used to heat a pre-compressed DT pellet to create the hot spot triggering ignition [1]. In addition, a study of fast electron transport dynamics helps in better understanding the TNSA mechanism of laser driven ion acceleration [2].

For the first time we have used proton probing to investigate fields arising from injection of relativistic electrons into dense matter. By employing the PW beam, very high energetic proton beams were produced, which could probe the interaction with very high spatial and temporal resolution. By using custom made foam targets, we could largely reduce the scattering of the probe beam and obtained field maps inside the foam target, clearly resolving fine filament structures.

Experimental setup

The experiment was carried out on the Vulcan Petawatt laser. A dual CPA configuration was used for the first time on this laser. We have used a small pickup mirror to extract a small part of the main beam. This second beam delivered around ~5% of the total energy at the interaction target. Using an f/6 parabola, this beam is focused down to a 10 µm focal spot, which delivered a peak intensity up to 2×10^{19} Wcm^{-2} on the foam targets of different densities and various compositions at an angle of incidence of 100. The PW beam is focused down to a 5 µm focal spot with a f/3 parabola. The PW arm is used to produce proton beam by irradiating a 25 µm Au foil. The schematic diagram of the experimental setup is shown in figure 1.

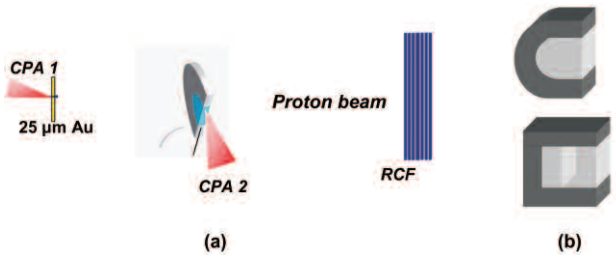

Figure 1(a). Schematic diagram of experimental arrangement. A dual CPA beam arrangement is used. A pickup mirror is used to extract ~5% of the total beam energy, which is used as interaction beam. The main PW beam is employed to produce high energy protons. (b) Diagram of different targets used.

The main problem to probe the high density region of the plasma is the scattering of the proton probe beam which can affect the spatial resolution of the diagnostic. To reduce the scattering we have used laminar foam targets: the thickness of the target in the transverse direction (proton probing axis) is made small to reduce the scattering. This is particularly important to resolve any fine filamentary structures arising inside the foam. The thickness of the foam in the laser propagation direction is around 1.5 mm or more, which is more than the penetration depth of fast electrons produced at these intensities [3]. Trimethylol Propane Triacrylate (TMPTA, $C_{15}H_{20}O_6$) foams were used. Foams were deposited in an Aluminium half washer of internal diameter of 1.5 mm and thickness 300 µm, with its side closed by a 8 µm plastic foil. Schematic diagrams of different targets are shown in figure 1(b). The front surface of the foam was coated with 75 nm of Au, with two aims. Firstly, the coating generates a radiation wave produced by the leading edge of the laser pulse which should help pre-ionising the

foam[4]. Moreover, by coating the interaction surface with Au we could assure that the electron source is the same in all the cases, irrespective of the variations in foam density or doping.

Foams of different densities, 20 mg/cc to 200 mg/cc, have been used to study the variation in electron propagation with densities. To study the effect of instabilities on electron propagation we have introduced electron density variation by doping the foam with medium (Cl) and high atomic number (Br) elements. We have used different percentages of doping. Finally we have used foams with Al foils embedded at a depth of 1 mm from the target surface, to study the effect of large density and resistivity gradients on hot electron propagation.

The interaction target was probed transversely by the proton beam. Thanks to the high-energy of the PW-produced protons, we could obtain images with very high spatial and temporal resolution. A double pass time slide arrangement has been used to adjust the time delay between the interaction and probing. Radiochromic film pack (RCF) were used as detector at a distance of 6 cm to obtain a magnification of around 16. As the protons with a particular energy deposit most of their energy at a particular depth (Bragg's peak), each layer of the RCF records the information of the interaction target at different stages owing to the difference in time of flight of protons of different energy.

Results

Figure 2 shows RCF images of the foam targets of density 100 mg/cc, at different times after the interaction. Times given on the top left corner are relative timing to the arrival of the peak of the pulse (within a couple of ps). We observe some very interesting features from these images. Figure 2(a) shows two dark lines at an angle of ~60°. This pair of lobe corresponds to the piling up of protons. This effect is starting around ~14 ps before the arrival of the peak of the pulse, where the intensity is still relatively low[5].

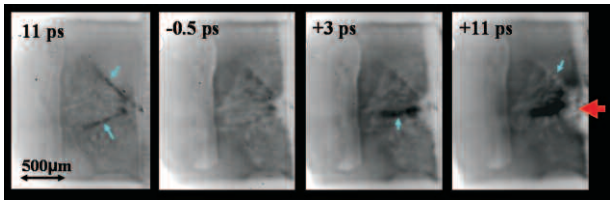

Figure 2. RCF images at different times after the interaction. Time shown on the top left is the relative timing to the arrival of the interaction beam. (a) and (b) Two angular lobes are observed in the earlier times with the rising edge of the pulse (c) and (d) strong collimated electric field is observed after the arrival of the peak of the pulse.

The pair of lobe indicates a localized electric field. At later times the lobes turns to white channels possibly due to existing magnetic field decaying on slower time scales. The lobes may be connected to a diverging electron cone injected into the target. The electron beam divergence is an important parameter in inertial confinement fusion as it determines the coupling of electrons to the hot spot[6].

Earlier studies used indirect methods like Kα imaging to study the electron beam divergence. To have some preliminary analysis, 3D particle tracing simulations were carried out. By introducing the fields corresponds to a diverging electron cone, we could obtain the simulation results matching with the experimental data. Further analysis is needed to confirm this.

Figure 3 compares the electron transport through pure and Br doped foam. 3(a) is the RCF image for 100 mmg/cc pure foam at different times whilst (b) is of 100 mg/cc, 30%Br doped foam. In the 100 mg/cc pure foam the two lobes are formed at an angle ~60°. In the case of Br doped foam we observe the lobes are developing at much higher angle of ~110°. For the Cl doping we found the lobe angle is ~72°. Further modeling and simulations are needed to study the effect of atomic number and or doping on fast electron divergence.

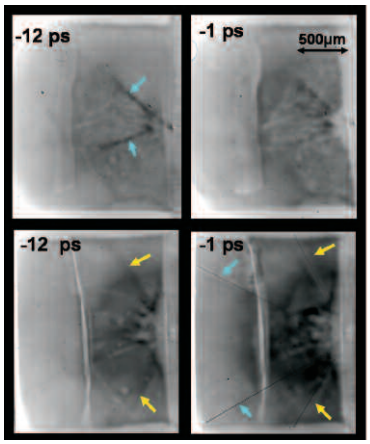

Figure 3. Comparison of electron transport through pure and doped foam. (a) RCF image of the 100 mg/cc pure foam. (b) images of the 100 mg/cc, 30% doped foam. In the doped foam two pair of lobes appear with different angle, may correspond to foam (medium Z) and Br (high Z).

After the arrival of the peak of the pulse, a dark feature is observed in the images, indicating a strong electric field near the axis (figure 2(c)). This electric field suggests injection of an electron jet. The velocity of the collimated jet is around ~0.6c possibly due to the strong electric inhibition inside the foam (this is more evident in pure foam where the atomic number is low). This is matching with the previous studies[7,8]. Initial electric inhibition results in the formation of a low resistivity channel due to ohmic heating and the resultant magnetic field generated at the edge of the electron beam channel inside the target leads to strong collimation[9].

Magnetic collimation

Magnetic focusing of fast electron beam is very relevant, as it can largely reduce the angular dispersion of fast electrons inside matter. Electron collimation has important implications for the fast igniter scheme[10] and other applications. Some of the data may provide evidence of magnetic focusing inside the target. Figure 4 shows the RCF images of 100 mg/cc, 30% Cl doped foam. It is

observed that at earlier times, with the arrival of the rising edge of the laser pulse, electrons are injected into the target with a large angle. As the beam propagates through the target, the current increases due to increasing laser intensity. This results in stronger magnetic fields. The magnetic field is azimuthal around the fast electron beam and acts to collimate it.

$$\frac{\partial B}{\partial t} = -\nabla \times E = \nabla \times (\eta J_{fast})$$

where η is the resistivity of the cold plasma, which depends on the atomic number and J_{fast} is the fast electron current density. At later stages the fast electron beam again start to diverge possibly due to the effect of beam filamentation instabilities.[11]

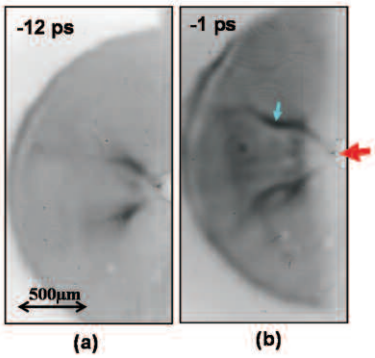

Figure 4. RCF images of 100 mg/cc, 30% Cl doped foam target indicating the magnetic focusing of the electrons. (a) Electron cone is injected into the target at a given angle in the earlier stage (b) at later stages the beam appears well collimated possibly due to magnetic collimation effects.

Filamentation

Relativistic electron beam propagation is largely affected by plasma instabilities. In the context of FI, the Weibel instability[12] could play a significant role, which might prevent the energy transport by the hot electron beam to be deposited in the hot spot in the compressed core of the pellet[13].

Figure 5 shows the RCF images of 50 mg/cc, 30% Br doped foam target. Very strong filamentation is observed. The filamentation is larger near the focal spot. As the density of the foam is relatively low we could observe filaments with reasonably good spatial resolution. The image shown is taken at 2 ps after the arrival of peak of the pulse. Filaments are much stronger along the laser propagation direction as the fast electron current density is higher in that region. This will result in strong current pinching as the return current become insufficient to balance the injected relativistic current. It is observed that the filaments along the laser direction appear white as the probe protons are expelled almost completely from this region. This may be due to very large magnetic field in the filaments.

Collimation of these filaments is also observed. It may be noted that the filaments close to the focal spot shows a more substantial collimation effect.

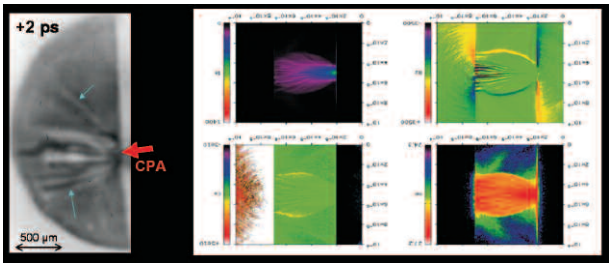

Figure 5. Images showing filamentation (a) RCF image of 50 mg/cc, 30% Br doped foam. Strong filamentation is observed. Also the image shows collimation and focusing of the filaments. (b) comparison with LSP simulation showing the distribution of temperature, magnetic field and hot electron density (image taken from ref.[14]).

Transport though interface

To study the propagation of fast electrons through large density and resistivity gradient, we introduced a 6 μm Al layer embedded inside the foam at a depth of 1 mm from the surface. Figure 6(a) shows the RCF data at different times. The target used is 100 mg/cc, pure foam. Via the proton deflection, it is observed that an electric or magnetic field is developed around the foil after the interaction. Indeed, since large density and resistivity gradients exist on both sides of the Al foil, a large magnetic field can be induced under this condition[14]. Figure 6(b) shows some LSP simulations (extracted from ref.[14]) of hot electron density and magnetic field distribution in such a situation.

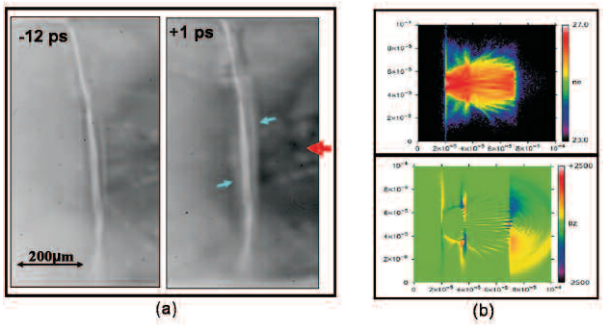

Figure 6. (a) RCF images show the effect of buried layer. An Al layer is embedded at a depth of 1 mm from the surface. RCF images are taken before and after the interaction. Field evolution is observed after the interaction. (b) LSP simulation shows the n_{hot} and B_z (extracted from ref.[14]).

Conclusions

For the first time we have obtained maps of the field distribution in the interior of laser-irradiated matter using the proton probing technique. Images with high spatial and temporal resolution are obtained. The data shows the variation in the injected fast electron cone with the laser intensity and density and or atomic number. Highly collimated electron jets are observed particularly with low Z material. Data shows strong filamentation possibly due to Weibel-like instabilities and provide indication of magnetic focusing. Information about the electron transport through density and resistivity gradient is

obtained. The results discussed here is from preliminary analysis of the data. Data shows good agreement with the existing models and simulations. Further, more advanced modeling and simulations are necessary to have an in depth knowledge of the causes of the features observed.

Acknowledgements
The authors would like to acknowledge the assistance of the staff of the Central Laser Facility at Rutherford Appleton Laboratory.

References
1. M. Tabak *et al*., *Phys. Plasmas*, **1**, 1626 (1994).
2. Fuchs *et al*., *Phys. Rev, Lett*., **91**, 255002 (2003).
3. A. R. Bell *et al*., *Plasma Phys. Contr. Fusion*. **39**, 653 (1997).
4. Jung *et al*., *Phys. Rev. Lett*., **94**, 195001 (2005).
5. C. Hernandez *et al*., RAL annual report, 200, 2004-05.
6. J. J. Honrubia *et al*., *Nucl. Fusion*, **46**, L25 (2006).
7. M. Borghesi *et al*., *Phy. Rev. Lett*., **83**, 21, 4310 (1999).
8. L. Gremillet *et al*., *Phys. Rev. Lett*., **83**, 24, 5015 (1999).
9. J. R. Davies *et al*., *Phys. Rev. E*, **59**, 6032, (1999).
10. M. Tabak *et al*., *Phys. Plasmas*, **1**, 1626, (1994).
11. J. C. Adam *et al*., *Phys. Rev. Lett.*, **97**, 205006 (2006).
12. E. S. Weibel, *Phys. Rev. Lett*., **2**, 83 (1959).
13. M. Honda *et al*., *Phys. Rev. Lett.*, **85**, 2128 (2000).
14. R. G. Evans, *High Energy Density Physics*, **2**, 35 (2006).